Effect of Sr substitution on rare earth mangnaites: $EuMnO_3$

A thesis submitted in the partial fulfilment of the requirement
For the degree of

MASTER OF SCIENCE

IN

PHYSICS

By

Shubhashree Swain

Roll No – 411PH2119

Under guidance of

Dr. Suryanarayan Dash

Dept. of Physics

National Institute of Technology, Rourkela

National Institute of Technology, Rourkela

CERTIFICATE

This is to certify that the thesis entitled "Effect of Sr substitution on rare earth manganite: $EuMnO_3$" submitted by Ms Shubhashree Swain in partial fulfilment for the requirement for the award of degree of Master of Science degree in Physics at National Institute of Technology, Rourkela is an authentic work carried out by her under my supervision and guidance in Department of Physics.

To the best of my knowledge, the matter embodied in the thesis has not been submitted to any other University/Institute for the award of any degree or Diploma.

Prof. Suryanarayan Dash
Dept. of Physics
National Institute Technology
Rourkela-769008

ACKNOWLEDGEMENT

On the submission of my thesis report titled “Effect of Sr substitution on rare earth manganite: $EuMnO_3$ ” I would like to convey my gratitude and sincere thanks to my supervisor Prof. Suryanarayan Dash , Department of Physics for his constant motivation and support during the course of my work in the last one year. I truly appreciate and value his esteemed guidance and encouragement from beginning to the end of this thesis. I am indebted to him for having helped me, shape the problem and providing insights towards the solution. I would also likely to acknowledge Ms Jashashree Roy and Mr Ranjit Kumar Panda for resistivity measurement.

ABSTRACT

An effort is made to study the effect of Sr (divalent atom) substitution in an otherwise antiferromagnetic insulator $EuMnO_3$. A series of samples have been prepared through solid state reaction route from the high purity constituent materials. The structural characterization is carried out by XRD with Retieveld analysis. Most of the samples in the series crystallises under orthorhombic structures with *Pnma* space group. With increasing concentration of Sr, the sample tends to more symmetric in nature. The SEM imaging renders the proper granular structures of the samples in the series. Moreover, a detail investigation is carried out for the transport features of the materials. The temperature dependence of resistivity shows unique features with varied concentrations of the Sr. With a lower concentrations favours the insulating state of the materials to that of semiconducting with increasing the content of Sr on the rare earth side of the parent manganite. The features are described in terms of the double exchange model with the support of structural parameters calculated for each material.

TABLE OF CONTENTS

Chapter-1 Introduction

1.1 Manganite

Manganite is a mineral, its composition is mainly MnO. These manganese based oxide materials, known as manganite , possess unique intrinsic properties of change in electrical resistance under the application of magnetic field, known as magnetoressistance can be expressed as

$$MR\% = \frac{(\rho_0 - \rho_H)}{\rho_0} \times 100$$

Where ρ_0 and ρ_H are the resistivity's in the absence and presence of magnetic field respectively. The doped $LnAMnO_3$ type or better known as ABO_3 type perovskite structure has cubic unit cell, where Ln represents the rare earth elements [1]. At the centre, Mn ions are surrounded by octahedral oxygen units known as the MnO_6 octahedral.

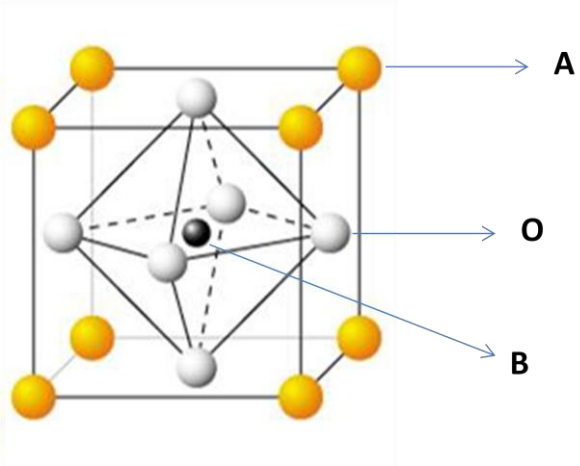

Fig. 1.1: Schematic diagram of perovskite (ABO_3) type structure of manganites

1.2 Half doped manganites:

Perovskite manganites with 50% of trivalent rare-earth ions of R^{3+} replaced by divalent alkaline-earth metal ions of A^{2+}, $R_{0.5}A_{0.5}MnO_3$ (R=La, Pr, Nd, etc;

A=Sr, Ca) known as half doped manganites, have been extensively studied and found to show many interesting electronic and magnetic properties. There are metal(M)-insulator(I) transition due to the double-exchange interaction (magnetic interaction between Mn^{3+} and Mn^{4+} that is caused by the hopping of eg electrons between the two partially filled d shells with strong on-site Hund's coupling), charge-ordering (CO) transitions due to the long-range Coulomb interaction among the carriers and antiferromagnetic transition due to the super exchange interaction, depending on the combination of R and A atoms. The above properties of manganites investigated, have been discussed by using various parameters such as average ionic radii $\langle r_A \rangle$ of R^{3+} and A^{2+}, tolerance factor t (which is a geometrical index defined as $t = (r_A+r_O)/2(r_{Mn}+r_O)$, where r_O is the ionic radius of O^{2-} and r_{Mn} is the average ionic radius of Mn^{3+} and Mn^{4+}), variance σ^2 etc. The 50% doping of the divalent metal cation on the rare earth site results a mixed valence with equal proportions of Mn^{3+} and Mn^{4+} ions in the system. From these classes, $La_{0.5}Sr_{0.5}MnO_3$ and $Pr_{0.5}Sr_{0.5}MnO_3$ compound with a larger $\langle r_A \rangle$, shows the metallic conductivity and a layered A-type AFM state where as $Nd_{0.5}Ca_{0.5}MnO_3$, $Pr_{0.5}Ca_{0.5}MnO_3$, $La_{0.5}Ca_{0.5}MnO_3$, and $Nd_{0.5}Sr_{0.5}MnO_3$ etc with a smaller $\langle r_A \rangle$, a CO insulating ground state has been obtained, in which Mn^{3+} and Mn^{4+} ions form two sublattice charge-exchange (CE)-type AFM structure. However, recently, the similar class of materials has been obtained by substituting a lower fraction of monovalent/alkali metal cation (Na^+, K^+ etc) on the same rare earth site. Due to charge neutrality, 25% of such alkali metal ion results a mixed valence of Mn^{3+} and Mn^{4+} ions (equal proportion) in the compound. Such mixed valence leads to several interesting properties in this system [1,2,3].

1.3 General Properties

The rare earth managnites is well known for their intrinsic but interesting physical phenomena and many researchers studied such class of materials for

several decades. Some important properties includes colossal magnetoresistance, Double exchange, phase separation, orbital and charge ordering etc [1].

1.3.1. Collosal magnetoresistance

Colossal Magneto resistance is a property of some materials, mostly manganese based perovskite oxides that enables them to dramatically change their electrical resistance in presence of magnetic field. The related formula has been already described in section 1.1. The magneto resistance of conventional materials enables changes in resistance of up to 5% but materials featuring CMR may demonstrate resistance changes by orders of magnitude. The magneto resistance, that means the resistance change induced by an external magnetic field, these phenomena observed, more or less in all metals and semiconductors. The particular MR phenomena to be described here are the gigantic decrease of resistance by application of magnetic field that is observed for the transition metal oxides and arise from the spin dependent scattering process of the conduction electron. Importantly the local spin and conduction electron are both of d-electron character. The external magnetic field cause the gigantic decrease of the resistivity around the curie temperature of that compound, below which the resistivity also show a steep decrease with decreasing temperature in zero field. Such gigantic negative magnetoresistance is called as colossal mangneto-resistance [1,2,3]. Many of the functional properties of these materials can be identified by this property. CMR effects in manganite arises due to spin disorder of conduction electrons which can be suppressed by application of magnetic field results in large magneto resistance.

1.3.2. Metal-Insulator Transition

This transition occurs in the vicinity of Para to Ferro transition. The temperature at which substance goes from insulator to metal is termed as Tp. When

magnetic field is applied to these materials then resistivity decreases sharply, particularly at the region of I-M transition

1.3.3. John Teller effect

The transition metal ions (Mn, Cu etc) have an active d-shell with five degenerate levels. It is well known that in empty space any direction or axis is same as any other. But in a crystal structure the ion is surrounded by a number of anions and the situation changes drastically, as the direction of the crystal axis more important than other directions. When the negatively charged ligands approach the central ion, the electrons of the latter are subjected to the repulsive force which is strongest in the approach direction of the ligands. Hence the energy of the orbitals which points in these directions is consequently increases. In manganites the Mn ion is surrounded octahedrally by six O; and their direction of approach coincide with the x, y, z axis which are precisely the direction along which the e_g orbitals (d_{x2-y2} and d_{z2}) are concentrated. Thus these e_g electrons are raised in energy and it occurs primarily due to electrostatic considerations between the d electrons and the surrounding negative ions. The t_{2g} (d_{xy}, d_{yz}, d_{zx}) orbitals which, points away from the O ions are lowered in energy.

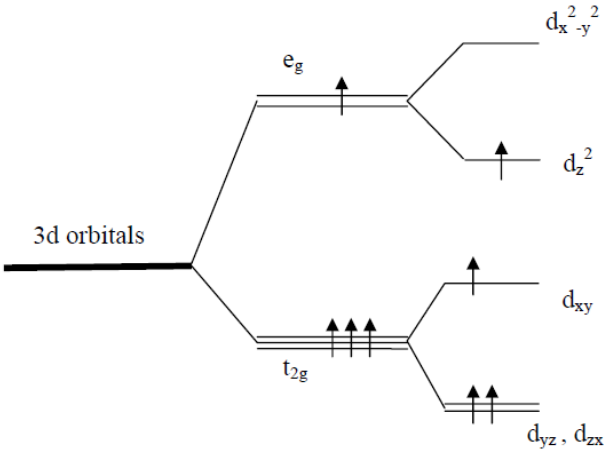

Fig1.2 Schematic representation of the crystal field effect of the d-levels of a transition metal ion in an octahedral crystal field.

Thus the five d- orbitals which are degenerate in a free metal ion are split into two set by octahedral ligand field. This is schematically shown in Fig. 3. This phenomenon of splitting of the inner d-orbitals by their surrounding in a chemical compound is known as crystal field splitting. d_{x2-y2} d_{z2} .

As explained in the previous paragraph, the splitting due to crystal-field effect lead to an e_g doublet and a t_{2g} triplet. For the Mn^{3+} (t_{2g}^{3} e_g^{1}) ion, the presence of a single electron in the doubly degenerate e_g levels can distort the octahedron such as to lift the degeneracy of the levels. The O ions around the Mn^{3+} ions readjust their location creating an asymmetry between the different directions leading to the removal of degeneracy. The lifting of degeneracy due to the orbital lattice effect is called the co-operative John Teller effect. This effect tends to occur because it is energetically favourable to spontaneously distort the lattice, thus removing the degeneracy. The MnO_6 octahedron is distorted in such a way that there are long and short Mn-O bonds. This is usually manifested in the form of a basal plane distortion with one diagonally opposite oxygen pair displaced outwards and the other pairs displaced inwards. Moreover, this John Teller distortion can both be static and dynamic. The former one occur in manganite with small hole density while the latter case occurs when the ion is not frozen in one distorted configuration but evolve among several configuration as a function of time [1].

1.3.4 Double Exchange Interaction

In perovskite manganites, depending upon the Mn-O-Mn bonding arrangements different magnetic configurations are possible in manganites. When both Mn-O bonds are covalent, the Mn–Mn separation is smallest. In this case each electron of the O ion spends majority of the time on different side of O ion. Since the two O electrons are anti-parallel, by semicovalence each couple

ferromagnetically with the net Mn ion spin with which it is predominately associated. Hence the two Mn ions couple antiferromagnetically.

However a special case arises when one Mn-O bond is covalent and other is ionic. Here the O ion is displaced towards the Mn ion with which it forms the covalent bond. Below transition temperature the covalent bond become semicovalent so that the net cation moment is associated with O ion. This moment due to the anion electron which participate less in a semicovalent bond may therefore couple antiferromagnetically to the net moment of the Mn ion which is coupled ferromagnetically via semicovalent bonding to the other anion electron. Now there is a direct exchange interaction between the moments of the anion and that of the neighboring Mn ion which is ionically bonded to it. Hence this Mn ion moment is anti-parallel to the anion moment, resulting in the ferromagnetic coupling of the two Mn ions. This phenomenon was used to explain the nature of magnetic interactions in stoichiometric $LaMnO_3$, which was shown to exhibit an A-type of antiferromagnetic structure, where two ab ferromagnetic planes are aligned antiferromagnetically [4].

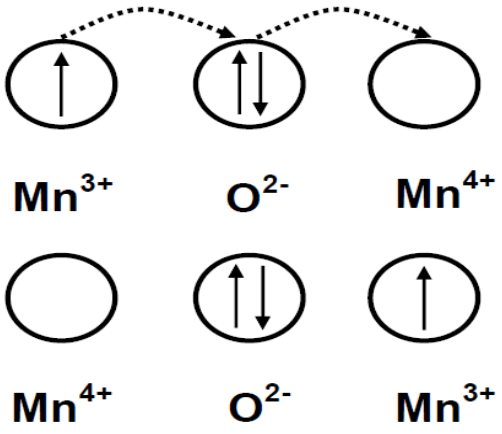

Fig1.3 Scematic representation of the double exchange process.

When an O ion is between Mn^{4+} and Mn^{3+}, the magnetic coupling is ferromagnetic. This mode of exchange interaction is known as double exchange interaction and was proposed by Zener [4]. This arises out of two fold

degeneracy (between Mn^{4+}-O-Mn^{3+} and Mn^{3+}-O-Mn^{4+}) in the ground state configuration. This phenomenon simply amounts to the simultaneous transfer of one e_g electron from the O the right Mn and from the left Mn to the O, such that there is a net transfer of an electron from left Mn to right Mn. The procedure is schematically shown in figure 2. This exchange mechanism is generalized by considering interaction between a pair of magnetic ions with general spin directions and the calculated transfer integral 't' is represented by

$$t = t_o \cos(\Theta/2)$$

where t_o is normal transfer integral which depends on the spatial wave functions and Θ is the angle between the spin directions . This phenomenon is different from the "super exchange interactions" where the coupling is proportional to cos (Θ) and the interaction are between the orbitally non-degenerate, localized t_{2g} orbitals.

1.3.5 Anti-ferro to ferro transition

In the ferromagnetic substances magnetic dipoles are present in domains. Inside the domains the magnetic dipoles are aligned without application of magnetic field. So they give rise to net non-zero magnetic moment and possess spontaneous magnetisation. In antiferromagnetic materials, magnetic dipoles are aligned oppositely gives rise to net zero magnetic moment. Here the temp Neel temp (T_N) above which they are paramagnetic and below which their behaviour is antiferromagnetic.

Under the application of simultaneous magnetic field and high pressure Antiferro to Ferro transition occurs. The temp of resistivity shows that width of transition and extent of hysteresis with pressure increase with magnetic field [5].

1.3.6 Application of CMR Manganite

- Magnetic field sensor using CMR effect in film.
- As a microwave CMR sensor magnetic field sensors used.
- Electric field effect devices using as ferroelectric gate.
- Bolometric uncooled IR sensor using metal insulator transition at curie temperature.
- Low temp. Hybrid HTS-CMR devices such as magnetic transducers and spin- polarised injection devices [5].

1.4 Aim of the Present work

After reviewing the earlier literatures [1,2,3], where most of the studies has been concentrated with La, Nd etc in manganites. In this present thesis we will try to study the effect of Sr doping on the rare earth side of the manganite in particular $EuMnO_3$ and its structural and other properties. As the Eu having zero effective magnetic moment, one can expect the interaction mechanism of Sr and its outcome in the compounds is more exciting. The Sr is doped here in accordance with the similar ionic radii to that of rare earth elements.

CHAPTER-2 SAMPLE PREPARTION

2.1 Solid State Route:

This preparation method is mostly followed in preparing the ceramic materials. It a process of direct mixing of the constituent powders in a stoichiometric ratios and heat treatment is given to the samples up to 1000^0-1500^0c with intermediate grinding. Here two factors are very important. Thermodynamic & kinetic factor. In thermodynamic factor, it involves whether a particular reaction should occur by considering change in free energy and in kinetic factor we determine what the rate in which reaction occurs is. During the process of preparation, it undergoes few intermediate processes; includes calcinations, pelletization, sintering etc [6].

2.1.1 Grinding

The main aim of the grinding is to make the mixture homogeneous and increase surface area of the mixture. Because of more surface area; more & more particles of powder are reacting and give good results of reactions. The surface area of reacting solid has a great influence on reaction rate. Since total area of contact between the grains of reacting solid depends on total surface area of grains. The process is that, the reactants have been weighted out in required amounts and mixed together. For manual mixing of small quantities, this may be done with an agate motor & pestle. Agate is preferable because it is hard & unlikely to contaminate with mixture & it is nonporous. After one hour mixing, the powders are intimately mixed & shows uniform colour [6].

2.1.2 Calcination

It is a process of heating a substance; but below melting point, causing loss of moisture. The mixture is generally calcined in the form of granules. The heating program to be used depends very much on reactivity of reactants. In the furnace,

the first stage of reaction must be decomposition of oxy salt. The mixture should be heated at appropriate temperature for few hours in controlled manner. If the stage is omitted, the mixture is heated directly at high temperature, it may cause sample to spit out from container. This calcination is generally done for few hours or even days and it also needs cooling [6].

2.1.3 Palletisation

It is a process of pressing the powder in uniaxial die press at room temperature by applying a force on it for increasing reaction rate. Here by pressing the reacting powder into pellet at high pressure, it increases the surface area. After pressing, many powder particles touch one another. The pellets are usually porous and crystal contents are not maximised. Depending upon our requirements sometimes hot pressing or cold pressing is required. In this method of palletisation, particles fit together better but densification is very slow [6].

2.1.4 Sintering

This process is used to increase the density of formed pellets. Generally after palletisation the pellets are around 60% dense & very weak bonding between grains. After sintering at high temp., the density and strength of pellet increases. In this process grain growth takes place [6].

2.2. Wet chemical route

The samples can also be made by wet chemical route, in which sample homogeneity can be maintained properly with a lower sintering temperature and time. In this method, the mixing of raw materials is in the form of solution resulting better homogeneity in the sample. The known methods include sol-gel, combustion, pyrophoric route etc.

2.3 Preparation of the series $Eu_{1-x}Sr_xMnO_3$

We have started with the parent composition as $EuMnO_3$. Stoichiometric ratios of the high purity materials of Eu_2O_3 (99.99%) and Mn_2O_3 (99.9%) from Alfa Aeiser are mixed together in a mortar and pestle. The detail process of making such materials is as follows:

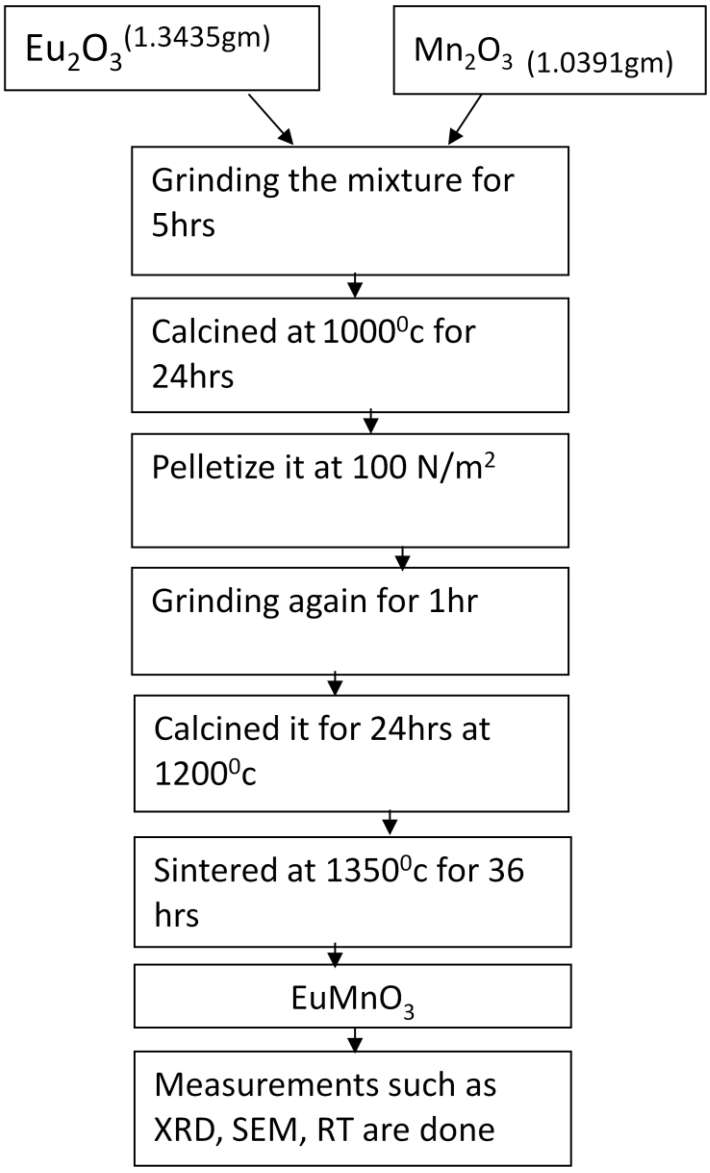

Other compounds in this seris have been prepared by following similar process like $EuMnO_3$.

Chapter-3 Characterization Techniques

3.1 X-ray Diffraction and Reitveld Analysis:

XRD is most common technique for the study of crystal structure and atomic spacing. It is also used for the identification of phase of a crystalline material and also provides information on unit cell dimensions. It is based on the principle of interference. X-ray diffraction occurs when there is a constructive interference between the monochromatic x-rays and the crystalline sample.

X-rays to be used are generated by a cathode ray tube by heating a filament to produce electrons. These electrons are then accelerated with the help of an applied voltage towards the target material. There are two types of X-ray depend upon how accelerated electron interacts with target material, and those are characteristic spectra and continuous spectra. In X-ray diffraction we use characteristic spectra; Cu-kα is widely used in XRD. In this case the diffraction occurs for the plane for which satisfies the Bragg's diffraction condition as $2d \sin\theta = n\lambda$. [5]

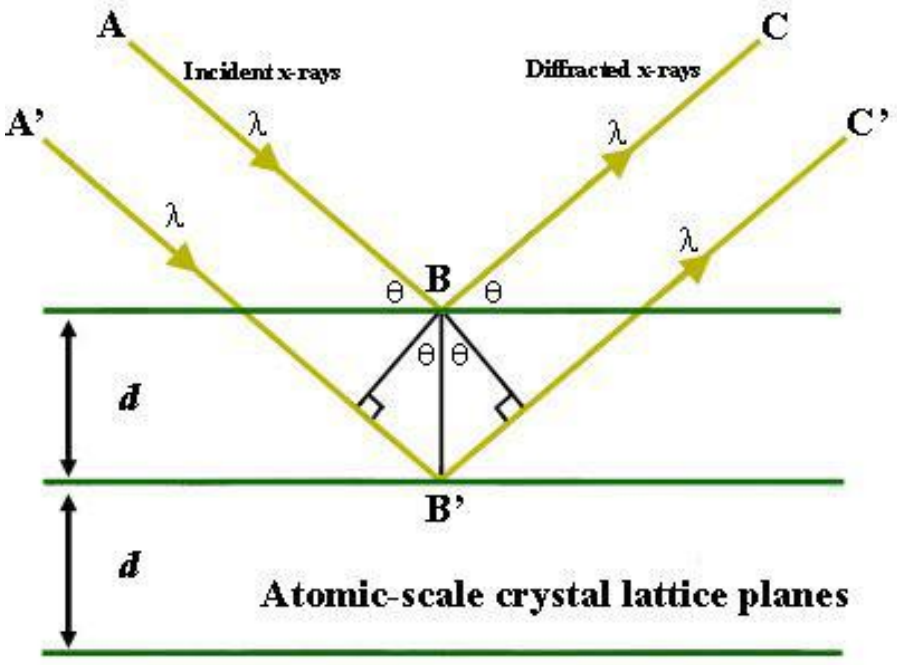

Fig 3.1The schematic representation of the XRD. The symbols used in the schematic are their usual meaning.

Rietveld refinement/Analysis is a technique devised by Hugo Rietveld for use in the characterisation of crystalline materials. The neutron and x-ray diffraction of powder samples results in a pattern characterised by reflections (peaks in intensity) at certain positions. The height, width and position of these reflections can be used to determine many aspects of the materials structure.

The Rietveld method uses a least squares approach to refine a theoretical line profile until it matches the measured profile (xrd data from the diffractometer). The introduction of this technique was a significant step forward in the diffraction analysis of powder samples as, unlike other techniques at that time; it was able to deal reliably with strongly overlapping reflections [7].

3.2 Scanning Electron Microscope imaging:

A SEM is a type of electron microscope that produces images of a sample by scanning it with a focused beam of electrons. The electrons interact with electrons in the sample, producing various signals that can be detected and that contain information about the sample's surface topography and composition. The electron beam is generally scanned in a raster scan pattern, and the beam's position is combined with the detected signal to produce an image. SEM can achieve resolution better than 1 nanometer. Specimens can be observed in high vacuum, low vacuum and in environmental SEM specimens can be observed in wet conditions.

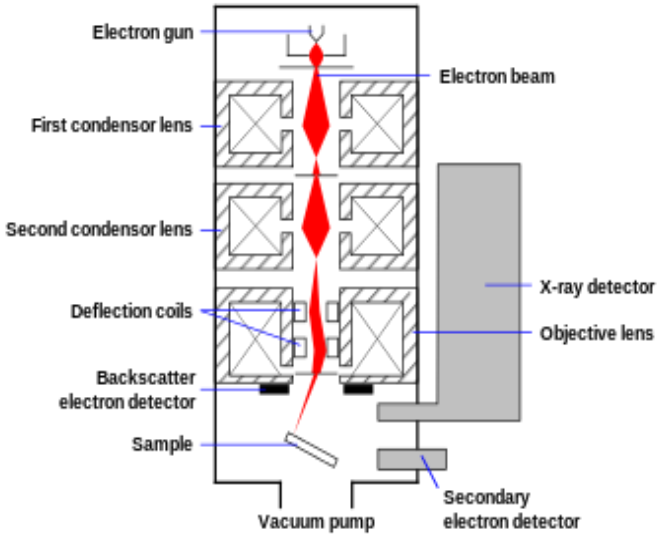

Fig3.2 Scematic representation of SEM used in this work

In the most common or standard detection mode, secondary electron imaging or SEI, the SEM can produce very high-resolution images of a sample surface, revealing details less than 1 nm in size. Due to the very narrow electron beam, SEM micrographs have a large depth of field yielding a characteristic three-dimensional appearance useful for understanding the surface structure of a sample. This is exemplified by the micrograph of pollen shown above. A wide range of magnifications is possible, from about 10 times (about equivalent to that of a powerful hand-lens) to more than 500,000 times, about 250 times the magnification limit of the best light microscopes. The SEM used in this work belongs to JSM 6480 LV-JEOL microscope [5].

3.3 Resistivity Measurement by four probe method:

Typically in most cases the resistivity of the specimen is measured by 4-probe method for better accuracy.

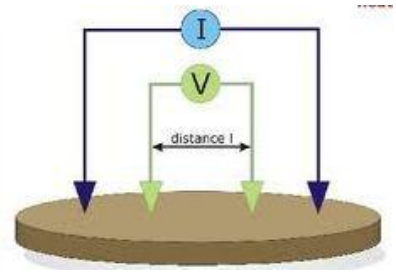

Fig3.3 Schematic diagram of the 4-probe method of resistivity measurement.

The four-point probe consists of four equally spaced metal tips with finite radius. A high impedance current source is used to supply current through the two outer probes, while a voltmeter measures the voltage drops across the inner two probes to determine the sample resistivity [5]. Typical probe spacing ~ 1mm. The temperature dependence of the resistivity is measured in a closed cycle refrigerator with temperature insert for varying temperatures.

Chapter-4 Results and Discussions

We have calculated the various controlling parameters (as discussed in the chapter 1) relating to the series of manganites and shown in the table:

COMPOSITION	$\langle r_A \rangle$ in Å	$\sigma^2 = \sum x_i r_i^2 - r_A^2$	$t = \frac{\langle r_A \rangle + \langle r_O \rangle}{\sqrt{2}(\langle r_B \rangle + \langle r_O \rangle)}$
$EuMnO_3$	1.230	0	0.909
$Eu_{0.9}Sr_{0.1}MnO_3$	1.251	0.0039	0.921
$Eu_{0.8}Sr_{0.2}MnO_3$	1.272	0.0070	0.934
$Eu_{0.7}Sr_{0.3}MnO_3$	1.293	0.0092	0.947
$Eu_{0.58}Sr_{0.42}MnO_3$	1.318	0.0107	0.962
$Eu_{0.5}Sr_{0.5}MnO_3$	1.335	0.0110	0.973
$Eu_{0.42}Sr_{0.58}MnO_3$	1.351	0.0107	0.983
$Eu_{0.2}Sr_{0.8}MnO_3$	1.398	0.0070	1.012

We observed that wth increasing in percentage of Sr; A-site cationic radius goes on increasing because ionic radius of Sr has more than Eu, which shows more towards a symmetric configurations. However the variances are not in order. Moreover the tolerance factor, is greater than one for high percentage doping of Sr (i.e. 0.8) which will give rise to some structural changes. So one can expect that with t tends to 1, the structure may modifies in the following way; Orthorhombic to rhombohedral to cubic. These parameters may act as a tool for describing the physical properties up to a greater extent. Note that, all the above parameters is calculated by taking the radii values of all the ions from reference 1.

4.1 Structural analysis by XRD

The XRD graphs of the series of samples are simultaneously depicted in fig4.1.

With higher and higher Sr concentrations, the samples tends to be in some higher symmetric state as identified from the less no of peaks.

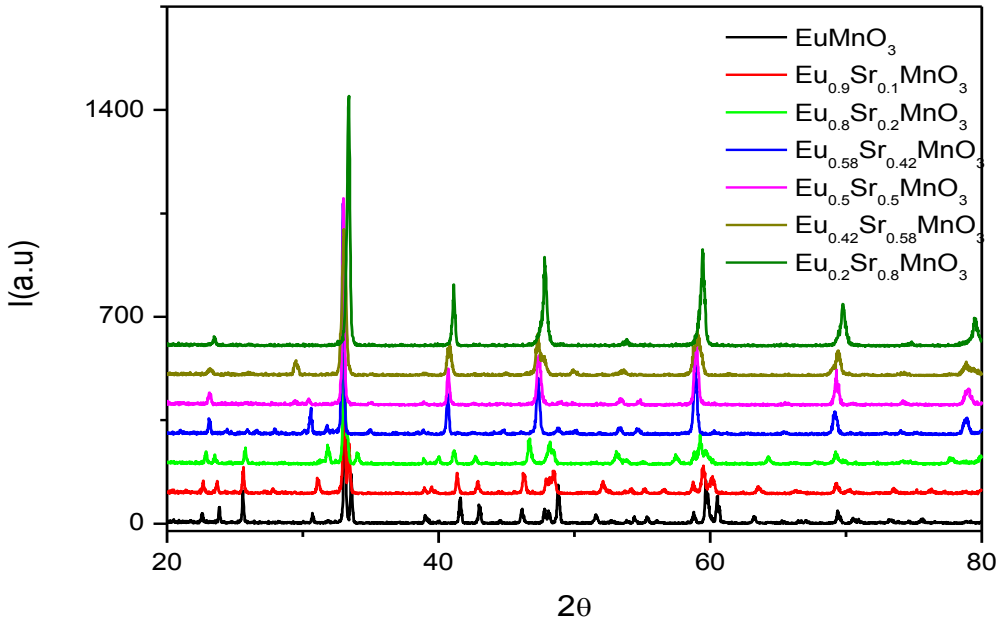

Fig4.1 Combined XRD pattern for the series $Eu_{1-x}Sr_xMnO_3$

We have done Reitveld analysis/refinement of the XRD data for structure determination for all samples, but a few representative graphs are shown below;

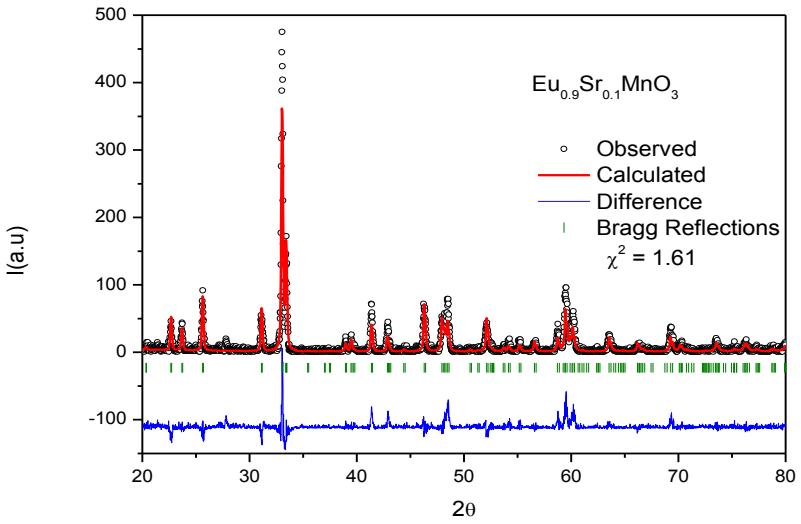

Fig4.2 Reitveld analysis of the XRD pattern for the sample $Eu_{0.9}Sr_{0.1}MnO_3$.(the black hollow symbol represents the observed data, the solid red line shows the calculated pattern, the blue line indicates the difference of the two pattern. However, the green solid lines give the Braggs reflections)

The samples crystallises in an orthorhombic structure with *Pnma* space group[8,9,10]. The refined structural parameters are tabulated bellow.

Atoms	x	y	z
Eu	0.0694(7)	0.25	-0.0136(11)
Sr	0.0694(7)	0.25	-0.0136(11)
Mn	0	0	0.5
O_1	0.5077(6)	0.25	0.0880(7)
O_2	0.2940(6)	0.0483(4)	0.7111(6)

a = 5.7457(5) ; b = 7.5052(9) ; c = 5.3609(5)
R_p = 38.3 ; R_{wp} = 45.7 ; R_{exp} = 37.2 ; Bragg R-factor =20.5; R_F factor = 13.6 ; χ^2 = 1.5. The symbols are their usual meanings.

Similar procedures has been followed for other samples and well documented in the following way as follows.

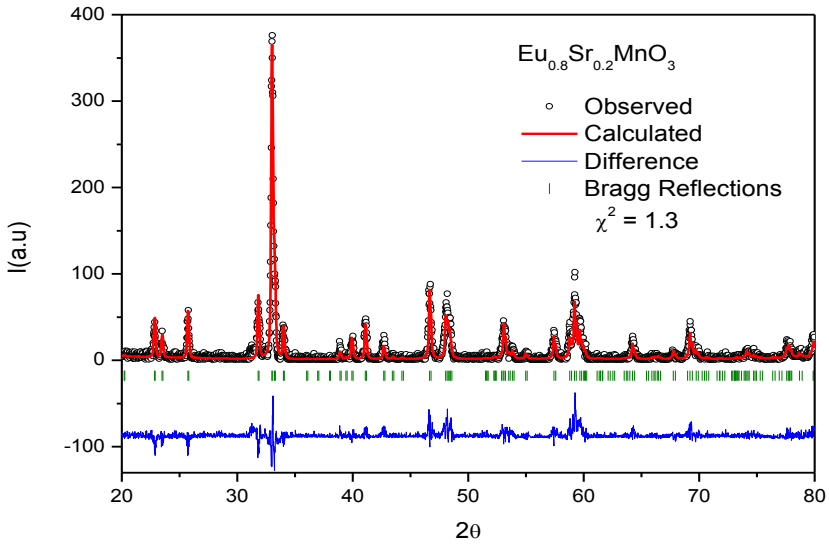

Fig4.3 XRD data with refinement pattern for the sample $Eu_{0.8}Sr_{0.2}MnO_3$.

The corresponding structural parameters are:

Atoms	x	y	z
Eu	0.567(6)	0.25	-0.0107(10)
Sr	0.567(6)	0.25	-0.0107(10)
Mn	0	0	0.5
O_1	0.4897(5)	0.25	0.0837(6)
O_2	0.02930(5)	0.0370(3)	0.7168(6)

a = 5.6220(5) ; b = 7.5685(8) ; c = 5.3899(5)

R_p = 36.2 ; R_{wp} = 43.9 ; R_{exp} = 38.1 ; Bragg R-factor =19; R_F factor = 13.3 ; χ^2 = 1.3

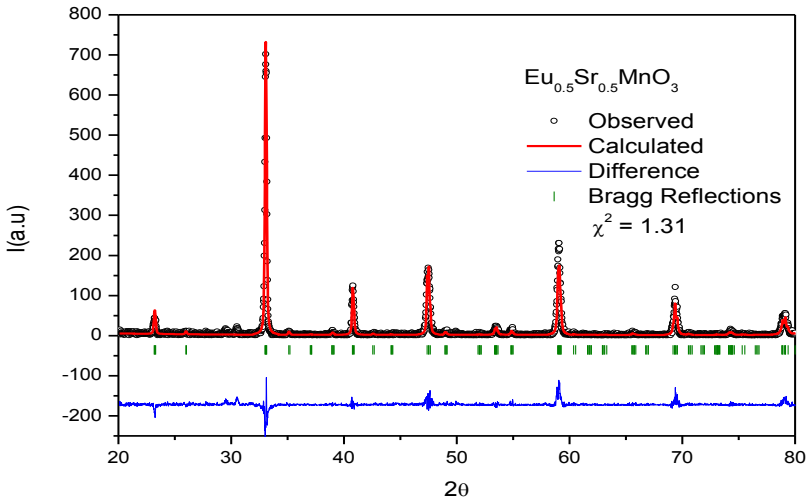

Fig4.4 XRD data with refinement pattern for the sample $Eu_{0.5}Sr_{0.5}MnO_3$.

Atoms	x	y	z
Eu	0.0198(7)	0.25	-0.0008(3)
Sr	0.0198(7)	0.25	-0.0008(3)
Mn	0	0	0.5
O_1	0.4962(5)	0.25	0.05874(13)
O_2	0.2785(11)	0.0287(5)	0.7294(8)

a = 5.4191(6) ; b = 7.6453(7) ; c = 5.4273(6)

R_p = 33.9 ; R_{wp} = 41.9 ; R_{exp} = 36.62 ; Bragg R-factor =15.09; R_F factor = 10.34; χ^2 = 1.31

From the detail Reitveld refinement, it was found that the samples are in single phase and stoichiometric.

4.2 SEM analysis:

We have done the imaging through SEM to figure out the granular structure of the entire sample which is depicted as follows with different magnifications:

$EuMnO_3$ $Eu_{0.9}Sr_{0.1}MnO_3$ $Eu_{0.8}Sr_{0.2}MnO_3$

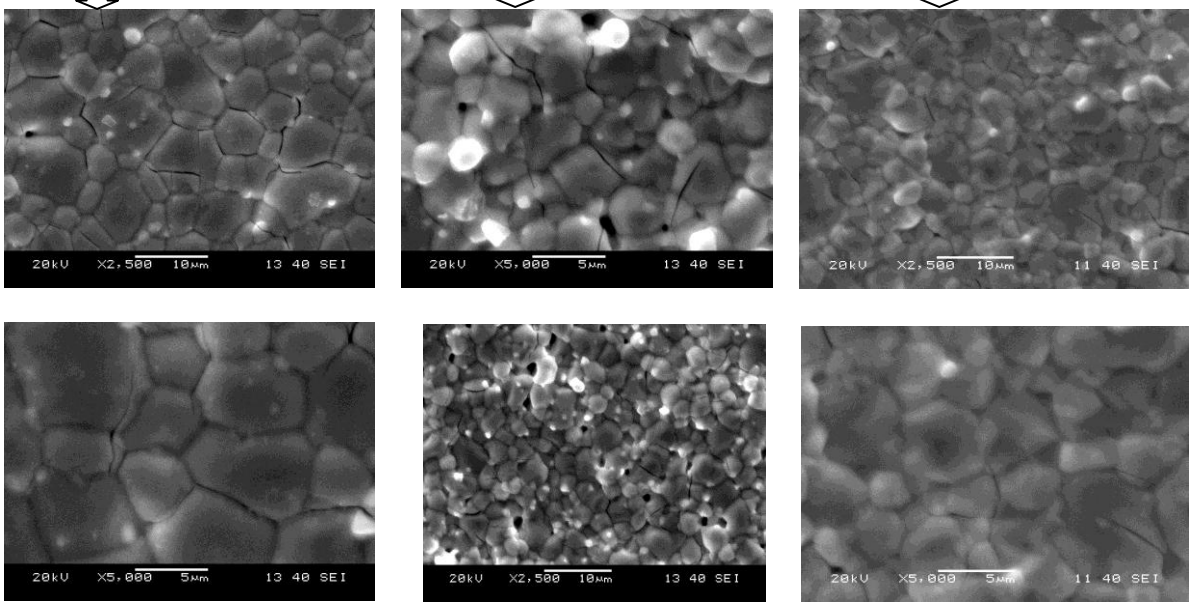

$Eu_{0.58}Sr_{0.42}MnO_3$

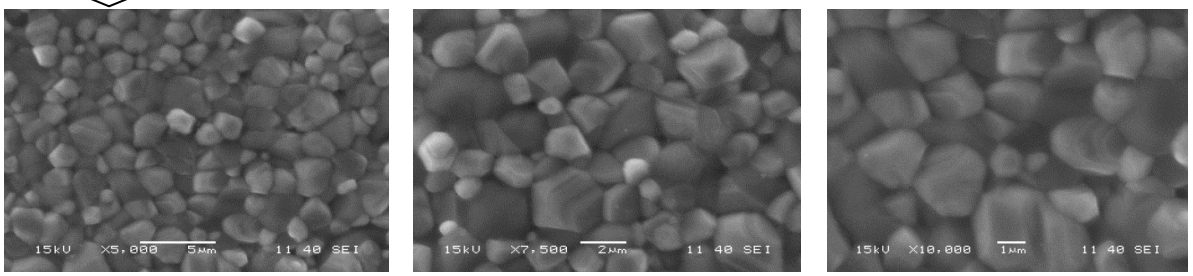

$Eu_{0.5}Sr_{0.5}MnO_3$

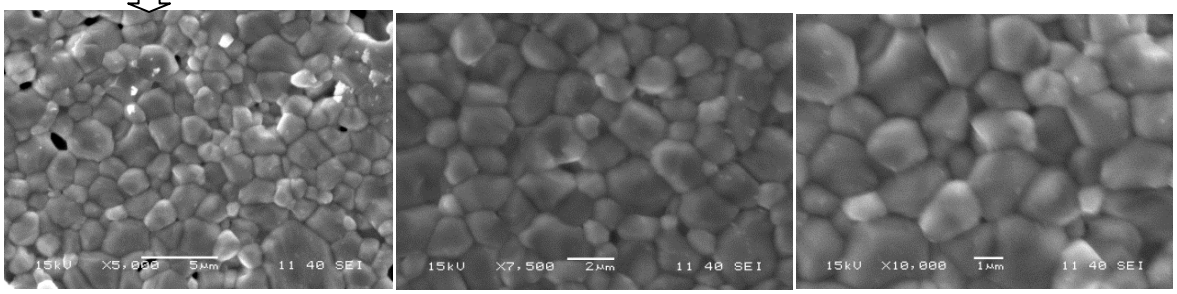

Fig4.5 SEM imaging of the series of smaples.

Most of the sample in this series shows a egular grannular pattern and has been clearly visible. In that case, the avarage size of the grannules is of teh order of ~1micron.

4.3 Temperature dependence of resistivity:

The transport behaviour has been studied for all samples in the series. For this resistivity is measured as functions of temperature from room T to lowest possible T in a closed cycle refrigerator with the usual four probe method. A few representative curves are shown below. The parent compound is a insulator. Fig4.6 a shows a complete insulating behaviour below some temp at which the resistivity is not measurable at a lower concentrations of Sr in $EuMnO_3$, however with increasing Sr makes the systems more semiconducting as depicted in fig4.6b

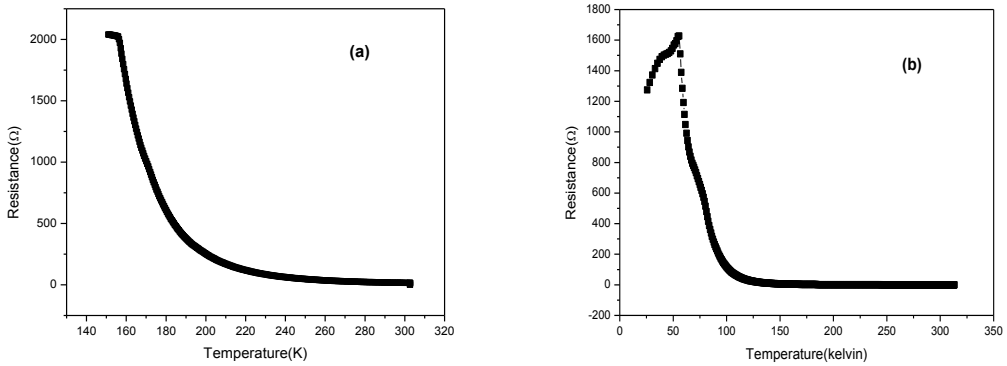

Fig4.6: The temperature dependence of resistivity of $Eu_{0.8}Sr_{0.2}MnO_3$ (a), $Eu_{0.5}Sr_{0.5}MnO_3$(b)

As shown in fig4.7, each curve log ρ vs 1/T is approximately linear for the higher temperature region, but it is curved with $d^2\rho/dT^2 > 0$ for higher x values in the lower T region. This indicates apparently $d\rho/dT < 0$, i.e temperature dependence is more rather semiconductive for the compositions. The value of ρ decreases with increasing composition x, i.e the electronic conductive increases with increasing x for this solid solution systems. The composition dependence of ρ on x corresponds to the evolution of Mn^{4+} states among the majority of

Mn^{3+} states [8,9,10]. The transport features are more like the compounds $LaMnO_3$ with its lower Sr concentrations[1], $Pr_{0.75}Na_{0.25}MnO_3$ in the family of rare earth mananites [11].

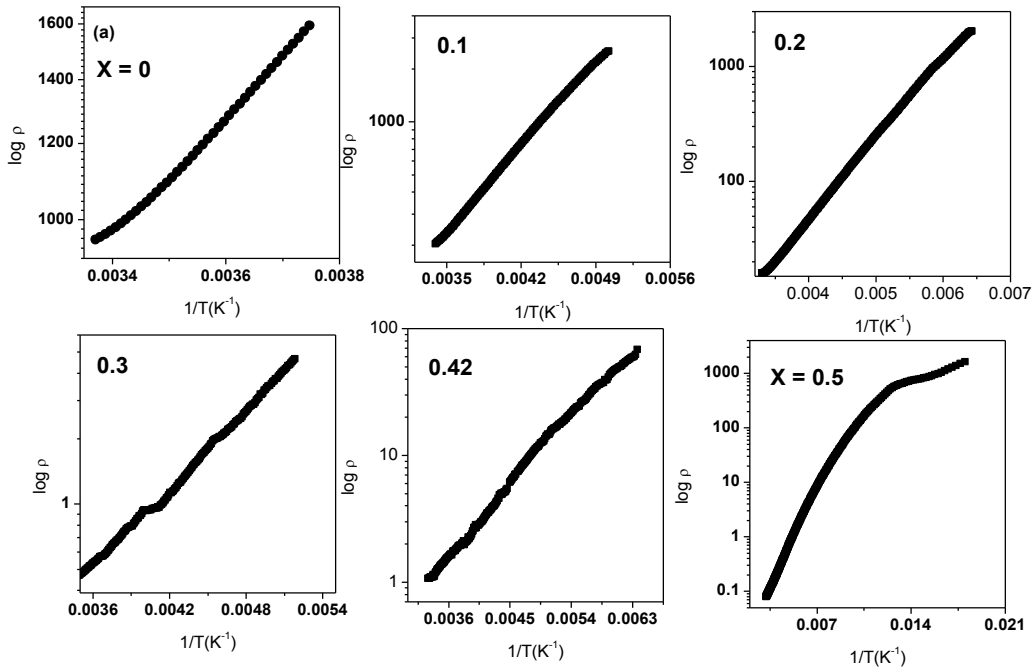

Fig4.12 shows the temperature dependence of resistivity ρ for polycrystalline ($Eu_{1-x}Sr_xMnO_3$) ($0 \leq x \leq 0.5$).

Chapter-5 Conclusions and scope of future work

To sum up, the series of samples has been prepared through solid state reaction route from the high purity constituent materials. to study the effect of Sr (divalent atom) substitution in an otherwise antiferromagnetic insulator $EuMnO_3$. The structural characterization is carried out by XRD with Retieveld analysis. Most of the samples in the series crystallises under orthorhombic structures with *Pnma* space group. With increasing concentration of Sr, the sample tends to more symmetric in nature. The SEM imaging renders the proper granular structures of the samples in the series. Moreover, a detail investigation is carried out for the transport features of the materials. The temperature dependence of resistivity shows unique features with varied concentrations of the Sr. With a lower concentrations favours the insulating state of the materials to that of semiconducting with increasing the content of Sr on the rare earth side of the parent manganite. The features are described in terms of the double exchange model with the support of structural parameters calculated for each material.

The future scope is concerned; one can study the detail electronic structures of this series to know the internal mechanism of the doping induced modifications in the physical properties.

References

1. Y. Tokura, Colossal Magnetoresistive oxides, Gordon and Breach Science publishers
2. C. N. R Rao;' colossal magnetoresistace, charge orsdering and related properties of mananganese oxides" world scientific publishing co.
3. E. Dagotto, 'Nanoscale Phase Separation and Colossal Magnetoresistance', Springer publishers.
4. C. Zener, Phys. Rev **82**, 403(1951)
5. www.wikipedia.org
6. A. R. West , Solid state chemistry and its applications, John willey sons, Singapore 1887
7. 'The Rietveld Method' Edited by R. A. Young
8. J. Z. Wang etal, Phys. Rev. B **76,** 104428(2007)
9. Y. Todokoro etal, Solid State Ionics **108**, 261(1998)
10. Y. Tomioka etal, Phys. Rev. B **80,** 174414(2009)
11. S. Dash etal, **113**, 17D912 (2013)